A Lower-Back Robotic Exoskeleton
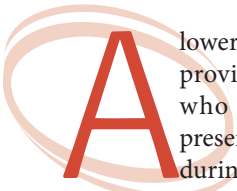
Industrial Handling Augmentation Used to Provide Spinal Support

By Ting Zhang and He (Helen) Huang

A lower-back exoskeleton prototype designed to provide back support for industrial workers who manually handle heavy materials is presented in this article. Reducing spinal loads during these tasks can reduce the risk of work-related back injuries. Biomechanical studies show that compression of the lumbar spine is a key risk factor for musculoskeletal injuries. To address this issue, we present a wearable exoskeleton designed to provide back support and reduce lumbar spine compression. To provide effective assistance and avoid injury to muscles or tendons, we apply a continuous torque of approximately 40 Nm on both hip joints to actively assist both hip abduction/adduction (HAA) and hip flexion/extension (HFE). Each actuation unit includes a modular and a

compact series-elastic actuator (SEA) with a clutch. The SEA provides mechanical compliance at the interface between the exoskeleton and the user, and the clutches can automatically disengage the torque between the exoskeleton and the user. These experimental results show that the exoskeleton can lower lumbar compression by reducing the need for muscular activity in the spine. Furthermore, powering both HFE and HAA can effectively reduce the lumbar spinal loading user experience when lifting and lowering objects while in a twisted posture.

Emergence of a Powered Lower-Back Exoskeleton

Manual material handling involves the actions of lifting, lowering, and carrying heavy materials in industrial environments. Lifting and lowering actions can significantly load the lumbar spine and increase an individual's risk of lower-back injury [1]. Work-related injuries increase industrial costs and,

more importantly, have a severe impact on a worker's quality of life [1]. There has been increasing research interest in the use of a wearable, powered exoskeleton to provide back support and reduce a user's risk of musculoskeletal injuries commonly resulting from material handling. Most existing back-support exoskeletons exert assistive forces between the torso and thighs to reduce muscular activity at the lower back and spinal loads to reduce the associated risk of injury [2].

Various exoskeleton prototypes have been developed for back support or load-carrying assistance, such as the Mk2 [2]–[5], PLAD [6]–[8], WSAD [9], backX [29], HAL Lumber Support [10], Power Assist Suit [30], Atoun Model A [31], HuMan [32], Axo-Suit [33], and Hyundai H-WEX 2 back-support exoskeleton for lift assistance [1]. The wearable exoskeleton design by Naruse et al. [11] can deliver an assistive force sufficient to lift 60 kg. Naruse et al. also demonstrated that this exoskeleton could considerably reduce the compression forces on the user's lower back as calculated by a simplified biomechanical model [1]. Kobayashi et al. developed a wearable, pneumatic exoskeleton to assist users carrying loads up to 30 kg [1]. A recent study by researchers at the University of California (UC), Berkeley, and UC, San Francisco, showed a 60% average reduction in electromyography (EMG) signals (i.e., muscle activations) at four of the most injury-prone lower-back muscle groups [1]. Electrodes were placed over four erector spinae muscle groups for eight test subjects, both wearing and not wearing the backX [29]. Not only do exoskeletons allow users to reduce their muscle activity; they also effectively reduce lumber compression in industrial handling activities, according to biomechanics modeling and analysis studies [12]–[14].

Commercial exoskeletons used for back support usually have powered hip joints that move in the sagittal plane. One limitation of the current back-support exoskeletons is that they do not provide back support in the frontal plane. A biomechanics study showed that individuals activate their gluteal muscles, which support HAA during lifting tasks, to maintain their balance and avoid twisting during asymmetric lifting of heavy objects [8]. Furthermore, asymmetric lifting and lowering actions are important factors in the incidence of lower-back pain and can cause prolapsed discs [15]. When individuals combine forward bending and lateral bending of their torso, the risk of work-related back injuries increases due to compressive forces exerted on the facet joints [16]. Based on epidemiological data, Snook et al. [17] showed that 33% of costs incurred by companies related to workers' lower-back pain is due to twisting and turning. A worker is usually instructed to avoid asymmetric lifting of heavy objects in the workplace to reduce lumbar spinal loading. However, it has been documented that losing symmetry during lifting and lowering tasks is more likely to occur, which may result in high loads on a worker's lumbar spine that can cause the worker's trunk to twist [1]. Thus, a lower-back exoskeleton with both sagittal and frontal plane back support is urgently needed to effectively reduce an individual's lumbar spinal loads due to twisting or losing symmetry while lifting and lowering heavy objects.

Recently, soft exoskeletons [18] have received research interest because, in contrast to traditional rigid exoskeletons with unbending support frames, they can be worn like clothing. Soft materials, such as textiles and elastomers, are used in the fabrication of soft exoskeletons, unlike the materials used in traditional rigid exoskeletons. However, to date, soft wearable exoskeletons have presented their own inherent limitations, such as an absence of weight-support functionality [19]. Given the current state of robotic technology, the implementation of a robotic lower-limb exoskeleton capable of biological levels of joint torque and velocity will likely introduce nonnegligible mass, rotational inertia, and possibly joint friction [20].

Safety is always the most important concern when it comes to the physical human–robot interaction of wearable lower-back exoskeletons; therefore, compliant actuators are preferred for exoskeletons. SEAs have been widely used in robotics because they offer a range of advantages over rigid actuators. SEAs have the ability to deform and take on various shapes, increasing adaptability and high-precision force control for enhanced user safety [21].

Building on previous research, this article presents a high-power, passively mechanical, and software-controlled actively compliant lower-back augmentation exoskeleton with four degrees of freedom that can assist in industrial material handling tasks. Our exoskeleton includes powered HAA and HFE. Each actuation unit includes a modular and compact SEA with a high torque-to-weight ratio. The unit provides mechanical compliance at the interface between the exoskeleton and the user to ensure user safety.

Exoskeleton Design

Structure

We developed a wearable exoskeleton to assist industrial workers when they lift and lower goods. The mechanical design of the powered lower-back exoskeleton is illustrated in Figure 1. It consists of three modules: the torso module, the powered hip exoskeleton, and the support leg. The articulation of the powered hip exoskeleton is achieved with four single-axis revolute joints: one for each HFE joint, mounted on the lateral arm, and one for each HAA joint. The torso module is a commercial extension orthosis thoracic spine brace (Cybertech Extension Orthosis Thoracic Spine Brace for Compression Fractures, Cybertech Medical, Thane, India). The prototype is designed to assist the user by applying opposite torques onto the thighs and torso. The exoskeleton backpack is secured to the user's body with pelvis and shoulder straps. Three cuffs per leg, with two at the calf and one at the thigh, attach the exoskeleton to the leg. To accommodate different users, the design includes several adjustable mechanisms such as telescopic structures in the thigh and shank and a sliding rail system at the pelvis. The powered hip exoskeleton, excluding the battery unit, has a total weight of 11.2 kg and conforms to wearers over a wide range of body sizes with
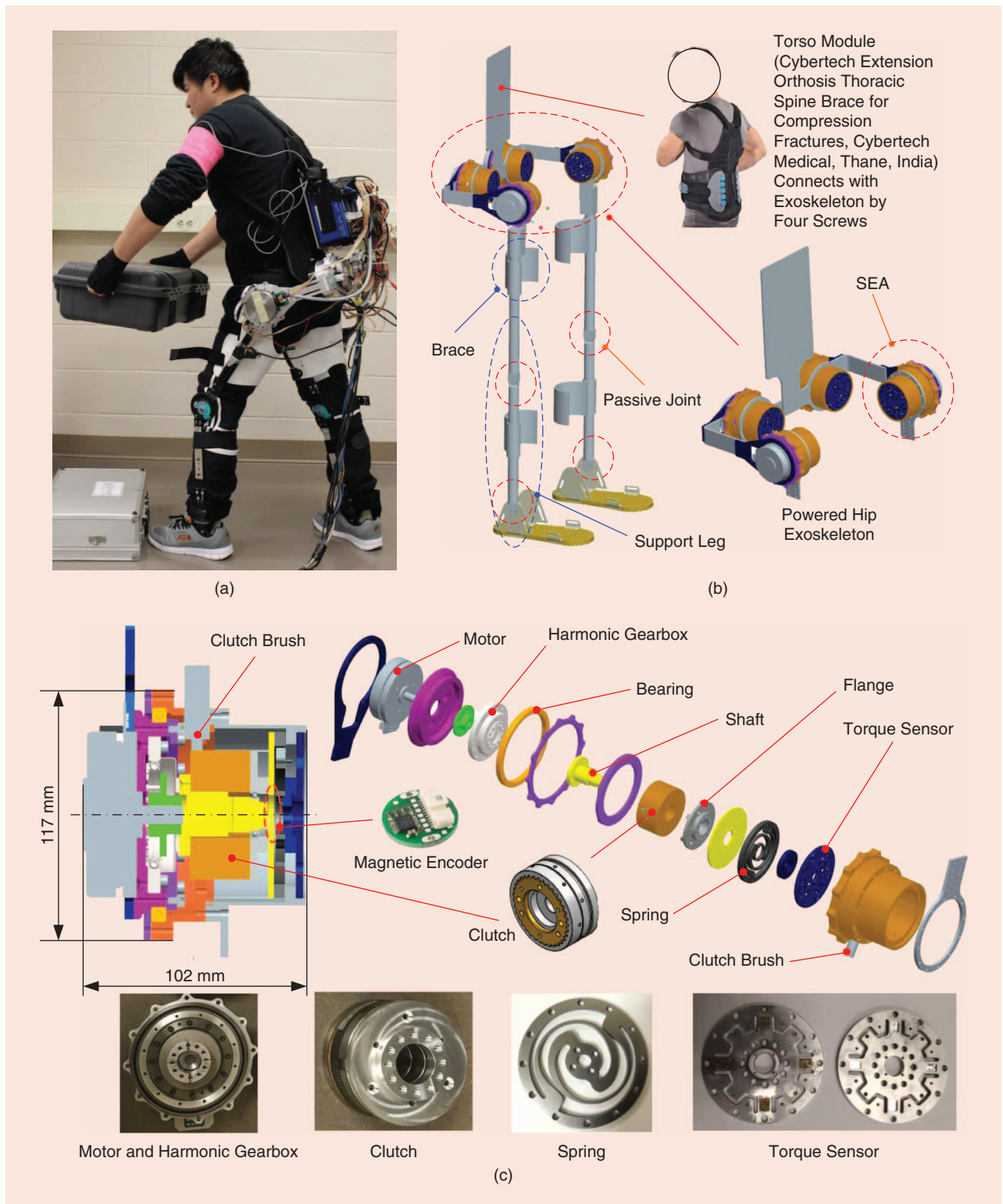
Figure 1. The lower-back robotic exoskeleton designs: the (a) exoskeleton prototype, (b) computer-aided design model of the lower-back robotic exoskeleton, and (c) main module of the SEA.

adjustable mechanisms. The support leg, including the passive knee and ankle and the link, can support the exoskeleton's weight.

Actuation

In our previous work, we introduced a compact SEA for a hip exoskeleton: NREL-Exo [22], [23]. In this article, the mechanical design parameters are enhanced by adopting a clutch to improve transparency and optimizing the torsion spring

design parameters to meet the stiffness and loading requirement. Each SEA module, including the kinematic and kinetic sensors, weighs approximately 1.8 kg, 0.6 kg of which is from the motor. The diameter is 122 mm, and the axial length is 63 mm. Table 1 lists the main features of the modular SEA.

1) *Actuator module*: Toxiri et al. [3] estimated that humans are able to generate more than 200 Nm to extend their lower back and hips, based on a biomechanical model and motion analysis. Our lower-back robotic exoskeleton was designed to provide about half of the extension torque (100 Nm), and the maximum output torque of the HFE actuator is set as 50 Nm [2]. The SEA is driven by a flat, brushless motor (EC 90 flat; Maxon Motor, Sachseln, Switzerland) and a harmonic drive gear (csd-25-100-2A-GR-BB; Harmonic Drive, Limburg, Germany). The output torque of the SEA is approximately 40 Nm, and the output velocity is roughly 150°/s.

2) *Clutch module*: A mechanical clutch (EC82/Z, electromagnetic tooth type clutch; Industrial Clutch Parts, Whaley Bridge, United Kingdom) is integrated in the SEA to automatically disengage and engage the transmission. The maximum bearing torque is 100 Nm, and the voltage is 24 V.

3) *Spring module*: The SEA was designed to have an angular series stiffness of 800 Nm/rad to allow 60 Nm of bidirectional torque loading. To minimize the torsion spring's dimensions and weight, the spring uses a monolithic disc shape. The monolithic disc-shaped design can reduce the spring's thickness, and it implies that the transfer of torque is between an outer annulus (external diameter of 85 mm) and an inner annulus (internal diameter of 12 mm). The material of the torsion spring is 50CrVA.

Sensing

To accomplish the compliant control scheme, the SEAs are equipped with numerous sensors. Each SEA has both kinematic (angular position, velocity, and acceleration) and kinetic (interaction force between the user's limb and exoskeleton) sensors:

- incremental encoder (4,095 pulse repetition rate; MILE, Maxon Motor, Sachseln, Switzerland) at each joint
- absolute magnetic encoders (RMB20; Rotary and Linear Motion Sensors, Komenda, Slovenia) at each joint
- inertial measurement units (IMUs) (VN-100S, Vectornav Embedded Navigation Solutions, Dallas, Texas) on the user's back.

A strain gauge-based torque sensor integrated into each SEA provides the torque measurement. The four strained beams are cross-shaped, and the rectangular groove is machined on each strained beam as an elastomer to sense strain. The strain gauges are connected in a full Wheatstone bridge for enhanced measurement accuracy. The linearity, hysteresis, and resolution of the torque sensor are 2.19%, 3.06%, and 0.41 Nm, respectively. Sensor noise was experimentally determined to be ±0.22 Nm, approximately 0.16% of the torque capacity.

Table 1. The main features of the modular SEA.

Features	Values	Unit
Continuous torque	40	Nm
Peak velocity	150	°/s
Series-spring stiffness	800	Nm/rad
Closed-loop control update frequency	2,000	Hz
Joint mass	1.8	kg

Embedded Electronics

The electrical hardware structure of the exoskeleton is shown in Figure 2. The embedded electrical system consists of a high-level subsystem and four joint lower-level subsystems. The high-level subsystem runs on a laptop. All high-level control algorithms are implemented in C# programming in Microsoft Visual Studio for real-time control. The joint lower-level subsystem consists of a 150-W commercial brushless motor driver (Copley Accelnet digital drive) and a mini digital signal processing (DSP) chip-based (TMS320F2808, Texas Instruments, Dallas) embedded control system. The functions of the joint lower-level subsystem include allowing motion control of the motor and providing feedback from the encoder, joint position sensor, and torque sensor signals to the high-level subsystem through the controller area network (CAN) bus. The lower-level control loop running on the DSP chip is updated at 2 kHz, and the control parameters are updated by the high-level controller at 100 Hz.

Control Approach

The back-support exoskeleton control system is based on a hierarchical architecture composed of a low-level control layer, which implements an admittance control, and a high-level control layer, which runs an assistive control that allows
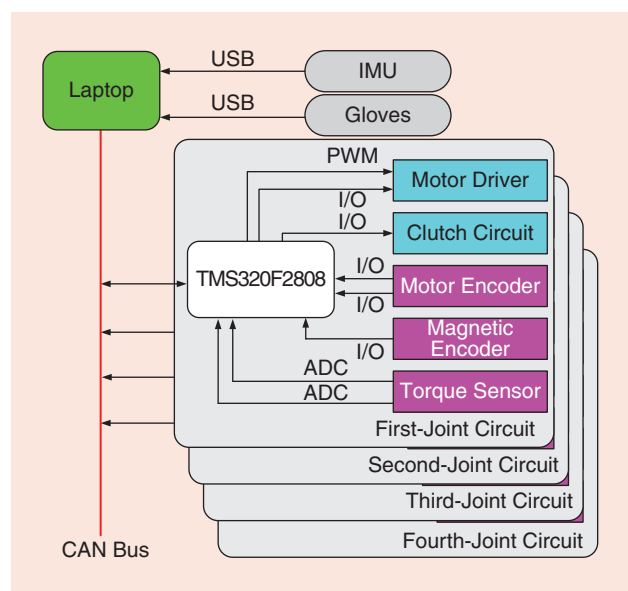
Figure 2. The electrical hardware structure. USB: universal serial bus; PWM: pulsewidth modulation; I/O: input–output; ADC: analog-to-digital converter.
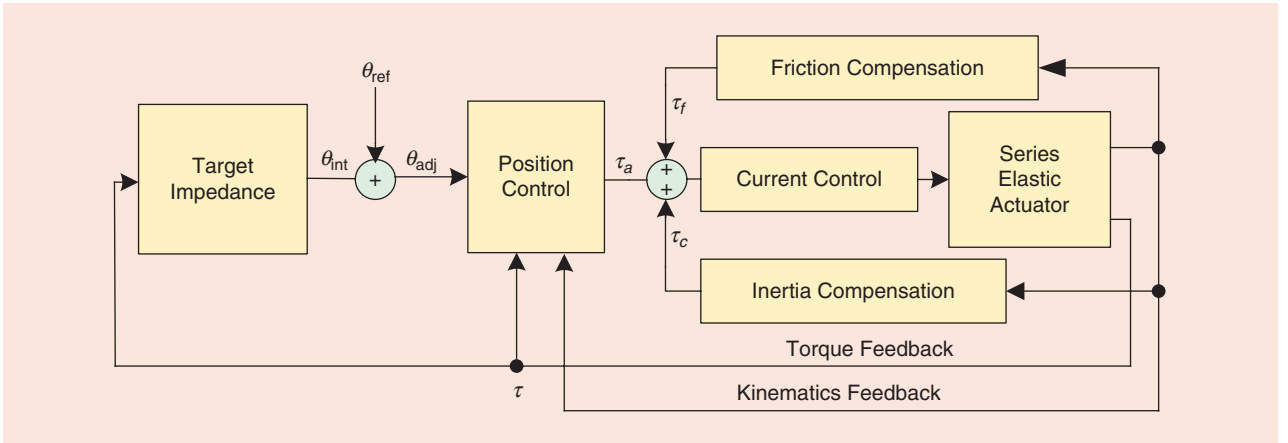
Figure 3. A block diagram of the low-level control.

the execution of all user assistance.

Low Level: Actuator Control

The low-level controller is based on admittance control

$$\theta_{\text{adj}} = \theta_0 - \frac{1}{K_d + sD_d}\tau, \tag{1}$$

where θ_0 is a desired angle and θ_{adj} is adjusted reference trajectory. The expression

$$\frac{1}{K_d + sD_d}\tau$$

is the angle related to the interaction torque τ between the exoskeleton and the wearer's joint. This angle is estimated using the virtual impedance parameters D_d and K_d of the exoskeleton, and it increases or decreases proportionally to the interaction torque between the wearer and the exoskeleton. An increase in the interaction torque indicates a greater difference between the trajectory of the wearer's limb and the trajectory of the exoskeleton. Figure 3 shows the block diagram of the low-level control, where

$$\theta_{\text{ref}} = \theta_0, \ \theta_{\text{int}} = \frac{1}{K_d + sD_d}\tau.$$

The variation in stiffness can be determined based on the performance of the wearer and the level of assistance exerted by the exoskeleton:

$$\begin{cases} K_{T+1} = K_T + \Delta K \\ \Delta K = \dfrac{\theta_0 - \theta}{\varepsilon\tau} \end{cases}, \tag{2}$$

where ε is a confidence factor in the interval [0,1] that is used to determine the stiffness to be applied at sample time T + 1. A low confidence factor means that partial or complete assistance should be provided, whereas a higher confidence factor indicates that the subject is capable of lifting and lowering with little or no assistance.

The physical model of an SEA [24] is

$$\begin{cases} B\ddot{\theta} = \tau_m - K(\theta - q) - D(\dot{\theta} - \dot{q}) - \tau_f \\ \tau = K(\theta - q) \end{cases}. \tag{3}$$

The SEA elasticity is modeled as a spring and a damper in parallel, where q is the link-side angle, θ is the motor-side angle, K is the SEA stiffness, D is the SEA damping, B is the motor inertia, τ_m is the motor output torque, τ is the elastic torque load on the SEA spring, and τ_f is the friction torque.

In general, the friction torque τ_f can be modeled as [25]

$$\tau_f = \left(\alpha_0 + \alpha_1 e^{-\left(\frac{\dot{\theta}}{v_s}\right)^2}\right)\text{sgn}(\dot{\theta}) + \alpha_2\dot{\theta}, \tag{4}$$

where α_0 is the coefficient of Coulomb friction, α_1 is the coefficient of Stribeck friction, v_s is the characteristic velocity of the Stribeck friction, and α_2 is the coefficient of viscous damping. The friction coefficients α_0, α_1, α_2, and v_s are identified experimentally.

By deviation of (3) in combination with (4) and (3), the SEA can be described as a function of τ:

$$\ddot{\tau} = \frac{K}{B}\tau_m - \frac{K}{B}\tau - \frac{D + \alpha_2}{B}\dot{\tau} - K\ddot{q}$$
$$- \frac{\alpha_2 K}{B}\dot{q} - \frac{K}{B}\left(\alpha_0\text{sgn}(\dot{\theta}) + \alpha_1 e^{-\left(\frac{\dot{\theta}}{v_s}\right)^2}\text{sgn}(\dot{\theta})\right). \tag{5}$$

In (5), the human motion is reflected in the term $K\ddot{q} + (\alpha_2 K/B)\dot{q}$, and the friction torque is related to the term

$$\frac{K}{B}\left(\alpha_0\text{sgn}(\dot{\theta}) + \alpha_1 e^{-\left(\frac{\dot{\theta}}{v_s}\right)^2}\text{sgn}(\dot{\theta})\right).$$

The current-control module has the following input terms

$$\tau_m = \tau_c + \tau_f + \tau_a, \tag{6}$$

where τ_c is the torque to compensate for the effect of the inertia, τ_f is the torque to compensate for the effect of the friction, and τ_a is the assistance torque. Substituting (6) into (5) yields

$$\ddot{\tau} = \frac{K}{B}(\tau_c + \tau_f + \tau_a) - \frac{K}{B}\tau - \frac{D + \alpha_2}{B}\dot{\tau} - K\ddot{q} - \frac{\alpha_2 K}{B}\dot{q}$$
$$- \frac{K}{B}\left(\alpha_0\text{sgn}(\dot{\theta}) + \alpha_1 e^{-\left(\frac{\dot{\theta}}{v_s}\right)^2}\text{sgn}(\dot{\theta})\right), \tag{7}$$

Table 2. The parameters of the joint.

Symbol	Quantity	Unit
Motor inertia (B)	0.0000668	$kg \cdot m^2$
Stiffness (K)	800	$N \cdot m/rad$
Damping (D)	0.563	$N \cdot ms/rad$
Stribeck velocity (v_s)	0.012	rad/s
Viscous coefficient (α_2)	0.431	$N \cdot ms/rad$
Bristle stiffness coefficient (α_0)	45	$N \cdot m/rad$
Bristle damping coefficient (α_1)	0	$N \cdot ms/rad$

Figure 4. The low-level control results for two different states of stiffness.

where τ_c is designed to ensure that the closed-loop system of the exoskeleton that interacts with the human leg has zero net torque:

$$\frac{K}{B}\tau_c - K\ddot{q} - \frac{\alpha_2 K}{B}\dot{q} = 0. \tag{8}$$

The variable τ_f is designed to ensure the friction force is completely compensated for:

$$\frac{K}{B}\tau_f - \frac{K}{B}\left(\alpha_0 \mathrm{sgn}(\dot{\theta}) + \alpha_1 e^{-\left(\frac{\dot{\theta}}{v_s}\right)^2}\mathrm{sgn}(\dot{\theta})\right) = 0. \tag{9}$$

The variables τ_c and τ_f are defined as

$$\tau_c = \frac{B}{K}\left(K\ddot{q} + \frac{\alpha_2 K}{B}\dot{q}\right), \tag{10}$$

$$\tau_f = \alpha_0 \mathrm{sgn}(\dot{\theta}) + \alpha_1 e^{-\left(\frac{\dot{\theta}}{v_s}\right)^2}\mathrm{sgn}(\dot{\theta}). \tag{11}$$

The parameters of the modular joint are shown in Table 2. The link mass and center of the mass were obtained from a three-dimensional simulation model. For the control application, it is necessary to identify the friction model of the SEA. The nonlinear function properly describes a static velocity torque (friction force) characteristic.

Figure 4 shows the low-level control results. The desired angle is set as zero, and the stiffness is set as 0.25 and 0.6 Nm/°. A healthy subject (male, 31 years old) wore the exoskeleton and performed movements of the left HFE with a frequency in the range of 0.1–2 Hz. The x axis corresponds to the hip joint angle, and the y axis corresponds to the interaction torque. The slope of the torque-angle plots is the stiffness. The corresponding static characteristic line according to the relevant stiffness value is denoted by the black line. The red line shows the desired stiffness. The root mean square of the stiffness tracking error is 0.47 Nm/°.

High Level: Assistive Strategy

As implemented in the high-level controller, a finite-state machine governs the behavior of the exoskeleton. During normal assistive handling, the exoskeleton is controlled by a high-level control scheme based on a finite-state machine and a low-level control scheme based on admittance control. Three states are defined for assisted handling: no loading, lift-
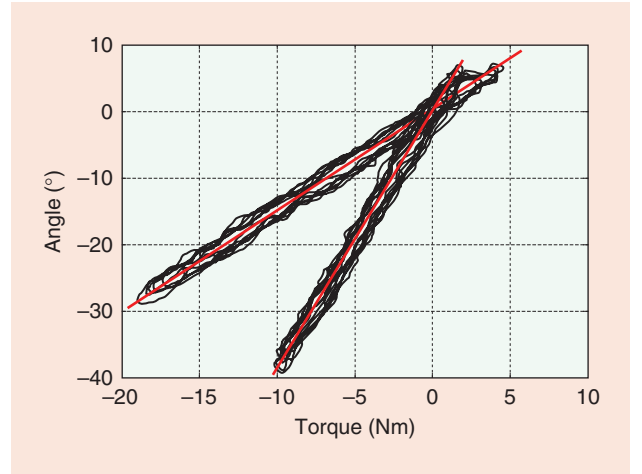
ing, and lowering. Each state consists of parameters describing the impedance of the four hip joints, including the joint stiffness (K), damping (D), and equilibrium angle (θ_0) as well as transition criteria. During operation, the states are concatenated to produce seamless assistance behavior.

Figure 5 shows the flow chart of the assistive strategy scheme. The finite-state machine uses the outputs from an IMU (VN-100S, VectorNav, Dallas, Texas), joint-torque sensors, and a pressure sensor (Force Sensitive Resistor 402, Interlink Electronics, Westlake Village, California) in a customized glove to transition between the three finite states of the state machine. We use the gloves' integrated force sensors to detect a load in the user's hand. When the gloves detect a load, the joints' clutches are engaged, and the exoskeleton will detect either a lifting or lowering task from the IMU and joint-torque sensor readings. When the HFE joint-torque sensors are rising-edge (i.e., the HFE joints' torque is increased due to the increment of weight) and the IMU is falling-edge (i.e., the pitch angle is increased), the finite state is lifting. When the HFE joint-torque sensors are rising-edge and the IMU is rising-edge, the finite state is lowering. In addition, when the HFE joint-torque sensors are falling-edge, the finite state is lifting [5], [6]. Table 3 shows the control parameters of each state. The stiffness in Table 3 is the initial value; these will be adjusted in real time during each task.

Performance of the Powered Lower-Back Exoskeleton

Figure 6 shows the user wearing the exoskeleton prototype. A healthy male subject participated in this study to evaluate the performance of our exoskeleton. This subject had no previous experience using the exoskeleton. The experimental protocol was approved by the Institutional Review Board of the University of North Carolina at Chapel Hill, and all human subjects gave written, informed consent before the experiment. Two experiments were conducted. Experiment 1 was performed to evaluate the capacity of the exoskeleton to assist lifting and lowering tasks. Experiment 2 aimed to evaluate

Table 3. The control parameters of each exoskeleton work status.

States	Joints	Clutch	Equilibrium Angle (rad)	Stiffness (Nm/°)	Damping
No loading	HFE	Off	–	–	–
	HAA	Off	–	–	–
Lifting	HFE	On	0	0.5	0
	HAA	On	0	0.5	0
Lowering	HFE	On	0	0.5	0
	HAA	On	0	0.5	0

whether both HAA and HFE assistance can be helpful for an asymmetric lifting-lowering task. The experiment required participants to lift a box from the floor to a full upright position, then lower it to the floor with a stoop-style motion (i.e., hip flexion, knee extension) [7]. The lifting-lowering tack was controlled at 2 s with a metronome. The subject performed this lifting-lowering motion for five sets, with 20 repetitions each. All repetitions were separated by approximately 5 min of rest. The subject was asked to choose a comfortable horizontal distance between his feet, provided it did not exceed 40 cm. The subject was not allowed to move his feet during the experiment because the direction of the pelvis might influence the lateral flexion and torsional torques [19].

To verify the capacity of the developed exoskeleton to ease the effort of the subjects during lifting and lowering tasks, EMG was collected from injury-prone lower-back muscle groups, including the left lumbar-erector spinae, right lumbar-erector spinae, left thoracic-erector spinae, and right thoracic-erector spinae muscles, to provide an estimate of general back muscle activity [1], [6]–[8]. Raw EMG signals were collected using a Delsys Bagnoli-8 system (Natick, Massachusetts) with a gain of 1,000 at a sampling rate of 1,000 Hz. For each lifting-lowering task, the start and end of the task were used to normalize each lifting-lowering motion to 0–100% [6]–[8]. For a statistical comparison, integrated EMG (iEMG) was used to evaluate muscles fatigue, which also has been used in previous work to evaluate muscle fatigue [6]–[8], [26], [27]. All EMGs were normalized to maximum EMG activity and then integrated with respect to the lifting-lowering task [6]–[8].

Experiment 1: Symmetric Lifting-Lowering Task

The human subject lifted and lowered a plastic box weighing 0, 5, 15, and 25 kg, depending on the load. The subject was asked to lift the box from floor to an erect standing posture and then lower it. The box had dimensions of 80 cm × 45 cm × 25 cm (width × depth × height) and was filled with weights to achieve the desired weight (5, 10, and 15 kg). The mass distribution of box was symmetric.

The subject lifted the box from the floor (the handles were 25 cm above the floor) at the front midsagittal plane (0°) to 72 cm above the floor, which was approximately the height of the person's knuckles when his arms hung vertically in a standing position [6]. He then lowered the box to the floor. Initial statistical analyses revealed no significant differences between the left and right lumbar-erector spinae EMG signals during the symmetric lifting-lowering task; therefore, data sets
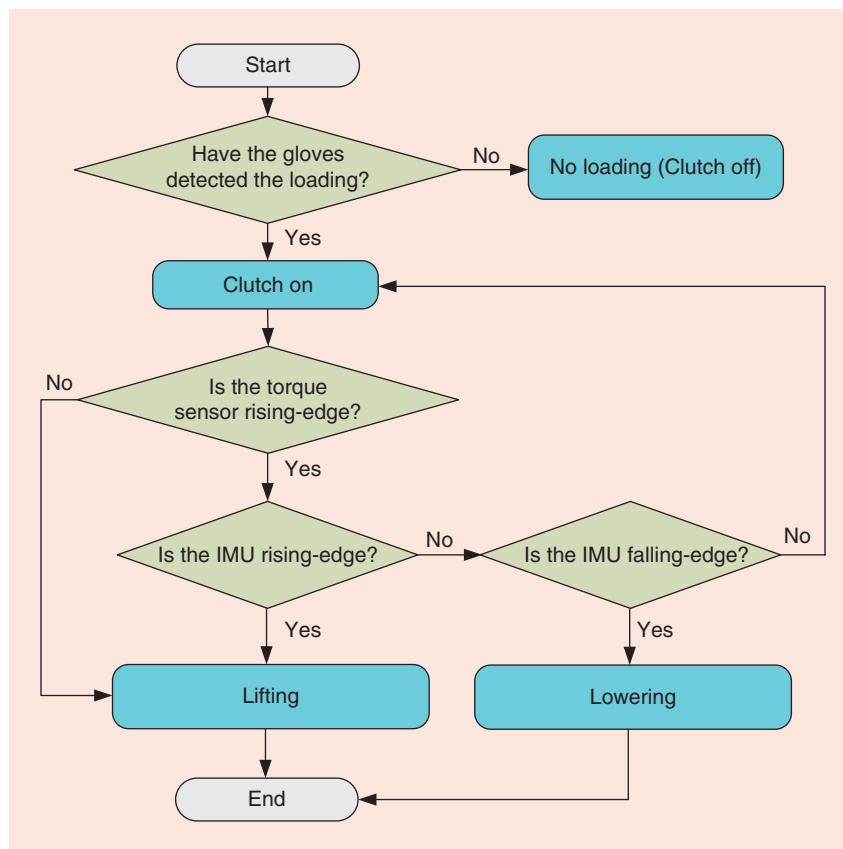

Figure 5. A flow chart of the assistive-strategy scheme. When the gloves detect a load, all of the joints' clutches are engaged, and then the exoskeleton will detect either a lifting or lowering task by the IMU and torque sensor. When the HFE joint-torque sensors are rising-edge (i.e., the HFE joints' torque is increased due to the increment of weight) and the IMU is falling-edge (i.e., the pitch angle is increased), then the finite state is lifting. When the HFE joint-torque sensors are rising-edge and the IMU is rising-edge, then the finite state is lowering. Finally, when the HFE joint-torque sensors are falling-edge, then the finite state is lifting.
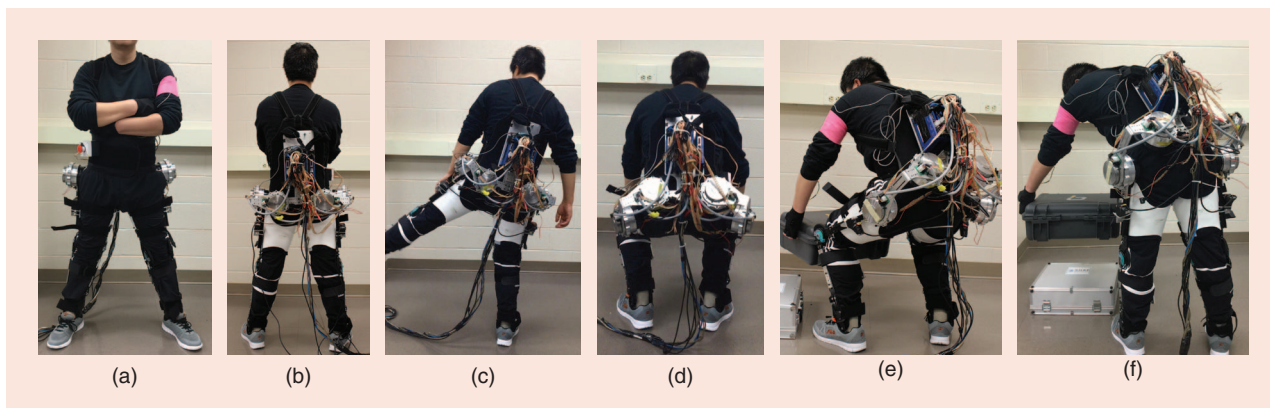
Figure 6. The user wearing the prototype and demonstrating different postures of a typical handling task. The (a) front and (b) back views, the (c) back view with a hip abduction, (d) symmetric lifting with a squat style, (e) asymmetric lifting with a squat style, and (f) asymmetric lifting with a stoop style.

showing both left and right EMG data were pooled and averaged for each test [12].

Figure 7 shows the kinematic analysis (joint angles) and dynamic analysis (assistance torque) results of both HAA and HFE joints during lifting-lowering scenarios. The angle profile of all cases remains almost the same, with only slight variations. The minimum HFE angle at the erect standing posture is around 0.2 rad. The velocity profile of all cases remains almost the same, with slight variations. From the angle plot and torque plots, we can see that, during lifting and lowering, the assistive torques at the HFE joints were positive. The assistive torque angles were well aligned. In both the lifting and lowering tasks, the exoskeleton provided assistance to help the wearer accomplish the task. The assistive torques varied with the box weights. The HAA joints provided a small amount of assistive torque during the symmetric lifting-lowering task.

Figure 7(b) shows the mean EMG for lifting and lowering 0, 5, 15, and 25 kg. When wearing the lower-back robotic exoskeleton, lower-back muscle fatigue (iEMG) was reduced from 16% ± 7%, 26% ± 8%, 48% ± 8%, 73% ± 4%, 15% ± 6%, 19% ± 8%, 27% ± 9%, and 47% ± 8%, for the 0-, 5-, 15-, and 25-kg lowering-lifting tasks, respectively. The results demonstrated that the proposed lower-back robotic exoskeleton significantly reduced lower-back muscle activity during the symmetric lifting-lowering task. These results are similar to the personal lift assistance device [6]–[8]. In line with work done by Abdoli et al., both left and right thoracic and lumbar-erector spinae's iEMGs were reduced between 14.4% and 27.6% when lifting symmetric loads of 5, 15, and 25 kg [8]. However, the relationship between the mean EMG and the net muscle torque is not straightforward because the EMG-to-contractile force relationships can be nonlinear.

Experiment 2: Asymmetric Lifting-Lowering Task

In this experiment, the subject was asked to asymmetrically lift a plastic box from the floor to an erect standing posture and then lower it to the original position with stoop style. The loads were positioned at 45°, approximately 15 cm from the body, as shown as Figure 6(f). The box had dimensions of 80

cm × 45 cm × 25 cm (width × depth × height) and was filled with weights to achieve the desired weight (15 and 25 kg). The subject performed the lifting-lowering task under three conditions: without exoskeleton, with the exoskeleton but without HAA joints assistance, and with the exoskeleton and with both HFE and HAA joint assistance.

Figure 8 shows the experimental results. Figure 8(a) and (b) includes the kinematics and dynamics for 15 and 25 kg, respectively. To show kinematic variety, we plotted the hip angle, torque, and mean center of mass (CoM) for three task conditions: without exoskeleton, with only HFE assistance, and with both HFE and HAA assistance. From these CoM plots, we can see that the CoM is tilted to the left (CoM is negative) and the HAA joints provide assistance to help the wearer shift his weight toward symmetry. The torque plots show that the exoskeleton HAA joints provide assistive torque to help the wearer shift his weight from the right to left side to achieve and maintain symmetry.

Figure 8(c) and (d) shows the mean EMG during the lifting-lowering task under three conditions. Dependent variables (left lumbar-erector spinae, right lumbar-erector spinae, left thoracic-erector spinae, and right thoracic-erector spinae muscles for 15 and 25 kg with three different task conditions) were expressed as means and standard deviations, as shown in Figure 7(e). For all asymmetric lifting-lowering tasks, greater reductions in muscle activity (iEMG) were observed with both HFE and HAA assistance compared to HFE assistance only. An example is shown in Figure 9, where the iEMGs of the left lumbar-erector spinae were measured at 51% ± 9%, 38% ± 7%, and 24% ± 8% without exoskeleton, with HFE assistance, and with both HFE and HAA, respectively.

Discussion and Conclusions

This article describes the design and control of a powered, back-support exoskeleton for industrial material handling. The proposed exoskeleton has powered hip joints to provide assistance to the user for both HAA and HFE, reducing lumbar spinal loading from lifting objects while in a twisted pos-
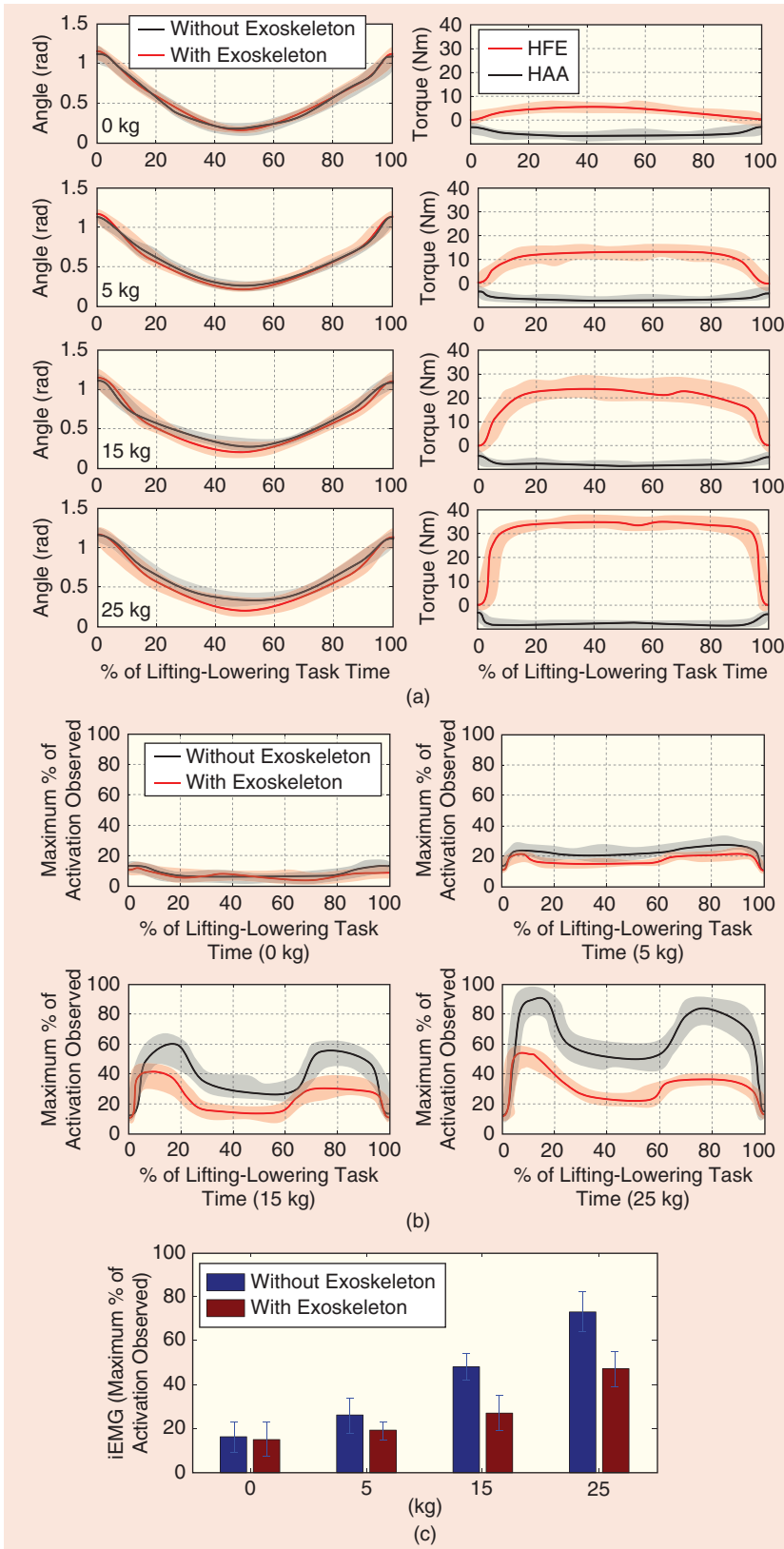
Figure 7. The symmetric lifting-lowering task. (a) The angle and torque of the hip joints for two conditions: without the exoskeleton and with the exoskeleton at 15 kg and 25 kg, respectively. (b) The mean EMG of the symmetric lifting-lowering task for two conditions: without the exoskeleton and with the exoskeleton at 15 kg and 25 kg, respectively. (c) The muscle activities (iEMG) are significantly reduced during the symmetric lifting-lowering task with the lower-back robotic exoskeleton's assistance.

ture. SEAs are used in the actuation modules, and the powered joints employ admittance control. This allows the device to achieve passive and software-controlled active compliance when interacting with the wearer. The exoskeleton is equipped with a clutch in the modular SEA that can automatically disengage the torque between the exoskeleton and the user to ensure safety.

Compared with other powered lower-back exoskeletons currently used for industrial material handling [3]–[11], this device offers several structural advantages. First, the high-power design along with simultaneous HFE and HAA actuation allows the exoskeleton to be potentially assistive to workers lifting, lowering, and carrying heavy objects. Furthermore, the high power supports the capacity of the lower-back exoskeleton to connect with other exoskeleton models, such as tool holding, power gloves, and upper-limb exoskeletons, to expand its application in industry and the workplace.

Our findings indicate that actively assisting individuals with lateral motion could potentially reduce the lumbar compression by decreasing the need for muscular activity around the lumbar spine during asymmetric lifting-lowering tasks. While the subject was using the proposed exoskeleton prototype with both HFE and HAA assistance, he exhibited muscle activity (iEMG) reductions during all symmetric and asymmetric lifting-lowering tasks.

The proposed lower-back robotic exoskeleton system has limitations. First, the weight of the exoskeleton prototype is relatively heavy, as there is a tradeoff between its ability to assist with loads and the weight of the design. Electromagnetic motors that combine high-reduction gears are the most common type of actuators on exoskeletons. Some exoskeletons adapt frameless motors [28] as actuators to reduce size and weight, but these systems are limited by the motor power and torque-to-weight ratio. Instead of using electromagnetic motors, it is possible to generate assistive forces
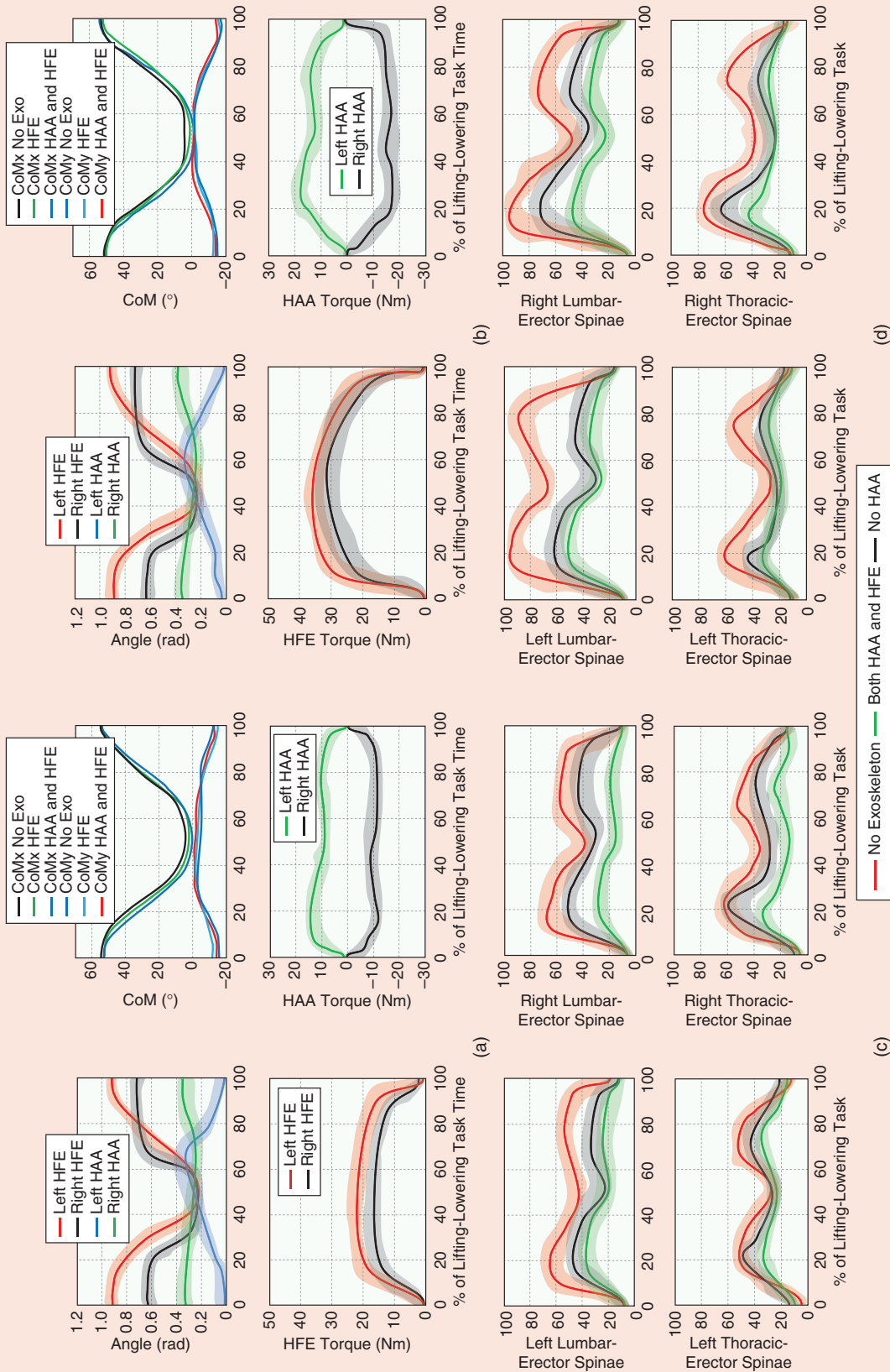
Figure 8. The asymmetric lifting-lowering task for three different task conditions: without the exoskeleton, with only HFE assistance, and with both HFE and HAA assistance. (a) and (b) The kinematics and dynamic data for 15 kg and 25 kg, respectively. (c) and (d) The mean EMG of three conditions. No Exoskeleton: without the exoskeleton; No HAA: with only exoskeleton HFE assistance; Both HFE and HAA: with both exoskeleton HFE and HAA assistance; LLES: left lumbar-erector spinae; RLES: right lumbar-erector spinae; LTES: left thoracic-erector spinae; RTES: right thoracic-erector spinae; CoMx no Exo: CoM at the x axis without exoskeleton assistance; CoMx HFE: CoM at the x axis with the exoskeleton with only HAA assistance; CoMx HAA and HFE: CoM at the x axis with the exoskeleton with both HFE and HAA assistance; CoMy no Exo: CoM at the y axis without exoskeleton assistance; CoMy HFE: CoM at the y axis with the exoskeleton with only HAA assistance; CoMy HAA and HFE: CoM at the x axis with the exoskeleton with both HFE and HAA assistance.
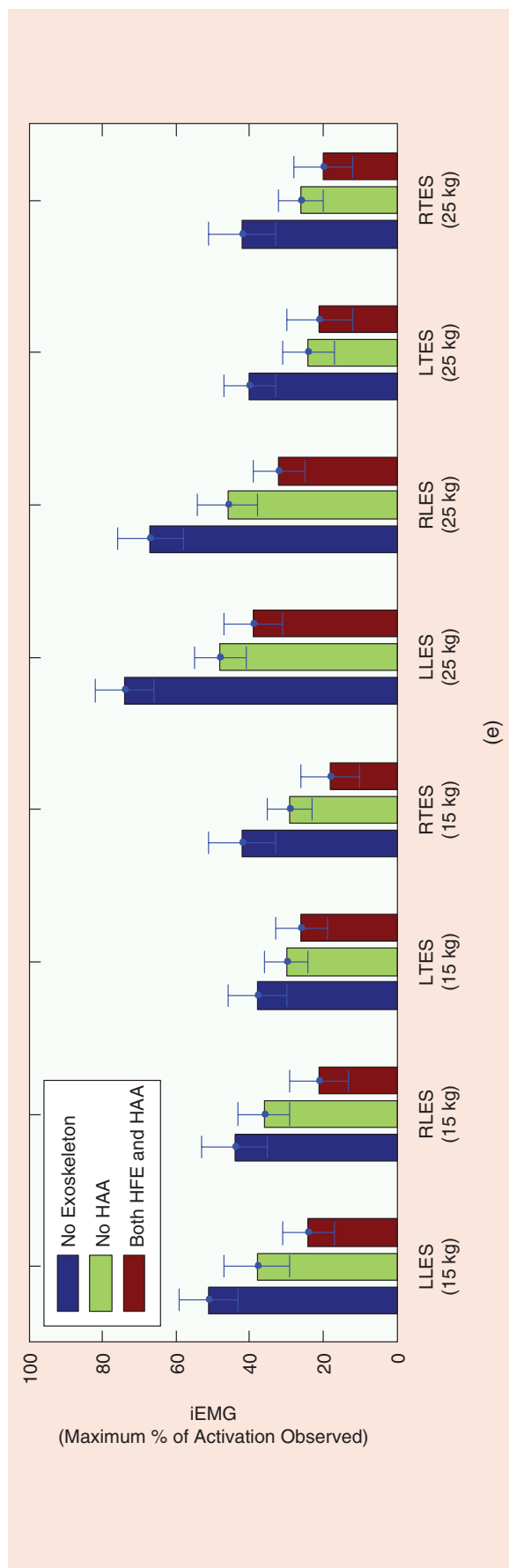
Figure 9. Muscle activities (iEMG) are reduced more when the proposed exoskeleton prototype is used with both HFE and HAA assistance than with only HFE assistance.

employing hydraulics or pneumatic muscles. Second, our exoskeleton prototype uses the passive knee and ankle joint to support the exoskeleton's weight. The clutch-able passive knee and ankle joints can be used to effectively support a load during a squat. Third, it is a challenge to accurately align rigid exoskeleton joints to a user's biological joints. The exploration of more possibilities for joint locations to solve the joint misalignment problem remains for future works. Additional research and engineering development are needed to make our device more useful for real-world load-carrying tasks.

Acknowledgments

References

[1] M. P. de Looze, T. Bosch, F. Krause, K. S. Stadler, and L. W. O'Sullivan, "Exoskeletons for industrial application and their potential effects on physical work load," *Ergonom.*, vol. 59, pp. 671–681, May 2016.

[2] S. Toxiri, A. Calanca, J. Ortiz, P. Fiorini, and D. G. Caldwell, "A parallel-elastic actuator for a torque-controlled back-support exoskeleton," *IEEE Robot. Automat. Lett.*, vol. 3, no. 1, pp. 492–499, Jan. 2018.

[3] S. Toxiri, J. Ortiz, J. Masood, J. Fernández, L. A. Mateos, and D. G. Caldwell, "A wearable device for reducing spinal loads during lifting tasks: Biomechanics and design concepts," in *Proc. IEEE Int. Conf. Robotics and Biomimetics (ROBIO)*, 2015, pp. 2295–2300.

[4] K. Huysamen, M. de Looze, T. Bosch, J. Ortiz, S. Toxiri, and L. W. O'Sullivan, "Assessment of an active industrial exoskeleton to aid dynamic lifting and lowering manual handling tasks," *Appl. Ergonom.*, vol. 68, pp. 125–131, Apr. 2018.

[5] S. Toxiri, J. Ortiz, and D. G. Caldwell, "Assistive strategies for a back support exoskeleton: Experimental evaluation," in *Proc. 26th Int. Conf. Robotics in Alpe-Adria-Danube Region (RAAD)*, 2017, pp. 805–812.

[6] D. M. Frost, M. Abdoli-E, and J. M. Stevenson, "PLAD (personal lift assistive device) stiffness affects the lumbar flexion/extension moment and the posterior chain EMG during symmetrical lifting tasks," *J. Electromyography Kinesiology*, vol. 19, pp. e403–e412, Dec. 2009.

[7] E. M. Abdoli, M. J. Agnew, and J. M. Stevenson, "An on-body personal lift augmentation device (PLAD) reduces EMG amplitude of erector spinae during lifting tasks," *Clinical Biomechanics*, vol. 21, pp. 456–465, June 2006.

[8] E. M. Abdoli and J. M. Stevenson, "The effect of on-body lift assistive device on the lumbar 3D dynamic moments and EMG during asymmetric freestyle lifting," *Clinical Biomechanics*, vol. 23, pp. 372–380, Mar. 2008.

[9] Z. Luo and Y. Yu, "Wearable stooping-assist device in reducing risk of low back disorders during stooped work," in *Proc. IEEE Int. Conf. Mechatronics and Automation*, 2013, pp. 230–236.

[10] H. Hara and Y. Sankai, "Development of HAL for lumbar support," in *Proc. Joint Fifth Int. Conf. Soft Computing and Intelligent Systems*

and 11th Int. Symp. Advanced Intelligent Systems (SCIS ISIS), 2010, pp. 416–421.

[11] K. Naruse, S. Kawai, H. Yokoi, and Y. Kakazu, "Development of wearable exoskeleton power assist system for lower back support," in *Proc. 2003 IEEE/RSJ Int. Conf. Intelligent Robots and Systems (IROS 2003)*, vol. 3, pp. 3630–3635.

[12] E. P. Lamers, A. J. Yang, and K. E. Zelik, "Feasibility of a biomechanically-assistive garment to reduce low back loading during leaning and lifting," *IEEE Trans. Biomed. Eng.* doi: 10.1109/TBME.2017.2761455.

[13] E. Lamers, A. Yang, and K. E. Zelik, "Biomechanically-assistive garment offloads low back during leaning and lifting," in *Proc. 41st Annu. Meeting of the American Society of Biomechanics*, Boulder, CO, 2017.

[14] H. Hara and Y. Sankai, "HAL equipped with passive mechanism," in *Proc. 2012 IEEE/SICE Int. Symp. System Integration (SII)*, 2012, pp. 1–6.

[15] H.-K. Kim and Y. Zhang, "Estimation of lumbar spinal loading and trunk muscle forces during asymmetric lifting tasks: Application of whole-body musculoskeletal modelling in OpenSim," *Ergonom.*, vol. 60, pp. 563–576, Apr. 2017.

[16] G. Aguirre-Ollinger, J. E. Colgate, M. A. Peshkin, and A. Goswami, "Design of an active one-degree-of-freedom lower-limb exoskeleton with inertia compensation," *Int. J. Robot. Res.*, vol. 30, no. 4, pp. 486–499, 2011.

[17] S. H. Snook, "The design of manual handling tasks," *Ergonom.*, vol. 21, pp. 963–985, Dec. 1978

[18] B. T. Quinlivan, S. Lee, P. Malcolm, D. M. Rossi, M. Grimmer, C. Siviy, N. Karavas, D. Wagner, A. Asbeck, I. Galiana, and C. J. Walsh, "Assistance magnitude versus metabolic cost reductions for a tethered multiarticular soft exosuit," *Sci. Robotics*, vol. 2, no. 2, pp. eaah4416, 2017.

[19] Y. Lee, Y. J. Kim, J. Lee, M. Lee, B. Choi, J. Kim, Y. J. Park, and J. Choi, "Biomechanical design of a novel flexible exoskeleton for lower extremities," *IEEE/ASME Trans. Mechatronics*, vol. 22, no. 5, pp. 2058–2069, 2017.

[20] S. A. Murray, K. H. Ha, C. Hartigan, and M. Goldfarb, "An assistive control approach for a lower-limb exoskeleton to facilitate recovery of walking following stroke," *IEEE Trans. Neural Syst. Rehabil. Eng.*, vol. 23, no. 3, pp. 441–449, May 2015.

[21] G. A. Pratt and M. M. Williamson, "Series elastic actuators," in *Proc. 1995 IEEE/RSJ Int. Conf. Intelligent Robots and Systems: Human Robot Interaction and Cooperative Robots*, vol. 1, pp. 399–406.

[22] T. Zhang, M. Tran, and H. H. Huang, "NREL-exo: A 4-DoFs wearable hip exoskeleton for walking and balance assistance in locomotion," in *Proc. 2017 IEEE/RSJ Int. Conf. Intelligent Robots and Systems (IROS)*, pp. 508–513.

[23] T. Zhang, M. Tran, and H. Huang, "Design and experimental verification of hip exoskeleton with balance capacities for walking assistance," *IEEE/ASME Trans. Mechatronics*, vol. 23, no. 1, pp. 274–285, Feb. 2018.

[24] H. Yu, S. Huang, G. Chen, Y. Pan, and Z. Guo, "Human–robot interaction control of rehabilitation robots with series elastic actuators," *IEEE Trans. Robot.*, vol. 31, no. 5, pp. 1089–1100, Oct. 2015.

[25] W. Chen, K. Kong, and M. Tomizuka, "Dual-stage adaptive friction compensation for precise load side position tracking of indirect drive mechanisms," *IEEE Trans. Control Syst. Technol.*, vol. 23, no. 1, pp. 164–175, Jan. 2015.

[26] E. F. Shair, S. A. Ahmad, M. H. Marhaban, and S. B. Mohd Tamrin, "EMG processing-based measures of fatigue assessment during manual lifting," *BioMed Res. Int.*, vol. 2017, p. 12, Feb. 2017.

[27] R. A. Malinzak, S. M. Colby, D. T. Kirkendall, B. Yu, and W. E. Garrett, "A comparison of knee joint motion patterns between men and women in selected athletic tasks," *Clinical Biomechanics*, vol. 16, pp. 438–445, June 2001.

[28] Y. J. Jeong, "Design of low profile, modular lower extremity exoskeletons," Ph.D. dissertation, Dept. Mechanical Eng., Univ. California, Berkeley, 2014.

[29] U.S. Bionics. (2003). backX: An effective and affordable exoskeleton that reduces the risk of work related back injuries. suitX. [Online]. Available: http://www.suitx.com/backx

[30] S. Toto. (2011, Sept. 21). Video: Kawasaki's power-assist robot suit helps human lift heavy objects. [Online]. Available: https://techcrunch.com/2011/09/21/video-kawasakis-power-assist-robot-suit-helps-humans-lift-heavy-objects/

[31] Atoun Inc. (2018). Power assist suit: Atoun Model A. [Online]. Available: http://atoun.co.jp/products/atoun-model-a

[32] HuMan. (2016). First testing of HuMan exoskeletons in Royo Group. [Online]. Available: http://www.humanmanufacturing.eu/2017/04/28/human-first-testing-exoskeletons-royo-group/

[33] Axo-Suit. (2018). Welcome to Axo-Suit. [Online]. Available: http://www.axo-suit.eu

Ting Zhang, Joint Department of Biomedical Engineering, North Carolina State University and University of North Carolina at Chapel Hill, Raleigh. E-mail: zhangt.hit@gmail.com.

He (Helen) Huang, Joint Department of Biomedical Engineering, North Carolina State University and University of North Carolina at Chapel Hill, Raleigh. E-mail: hhuang11@ncsu.edu.